Electrophysiology and data analysis

Synaptic currents were recorded in HL-3 saline from muscle 6 in segment A2 using a two-electrode voltage clamp[28]. For EJC recordings, stimuli consisted of 0.2 ms pulses delivered at 1 Hz from an isolated pulse stimulator (AM systems 2100), gated by pClamp software (Axon Instruments). Intracellular glass microelectrodes were filled with 3 M KCl (voltage monitor electrode, resistance 7–10 MΩ) or saturated potassium citrate and 3 M KCl (current injection electrode, resistance 18–25 MΩ). Data were acquired from muscles clamped at −70 mV, using an Axoclamp 2B amplifier (Axon Instruments), and recorded with pClamp software. Data were filtered at 1 kHz before analysis. EJC amplitude was determined from 22–25 contiguous stimuli, and mEJC parameters were measured from one to two 41-s records, using the minianalysis software (Jaejin Software). Differences between means were compared using either *t*-tests (paired comparisons) or analysis of variance (ANOVA; multiple comparisons) in Microsoft Excel or SigmaPlot.

Received 26 November 2001; accepted 21 February 2002.

1. Bailey, C. H., Bartsch, D. & Kandel, E. R. Toward a molecular definition of long-term memory storage. *Proc. Natl Acad. Sci. USA* **93,** 13445–13452 (1996).
2. Curran, T. & Morgan, J. I. Fos: an immediate-early transcription factor in neurons. *J. Neurobiol.* **26,** 403–412 (1995).
3. Davis, G. W., Schuster, C. M. & Goodman, C. S. Genetic dissection of structural and functional components of synaptic plasticity. III. CREB is necessary for presynaptic functional plasticity. *Neuron* **17,** 669–679 (1996).
4. Sheng, M., McFadden, G. & Greenberg, M. E. Membrane depolarization and calcium induce c-fos transcription via phosphorylation of transcription factor CREB. *Neuron* **4,** 571–582 (1990).
5. Yin, J. C., Del Vecchio, M., Zhou, H. & Tully, T. CREB as a memory modulator: induced expression of a dCREB2 activator isoform enhances long-term memory in *Drosophila*. *Cell* **81,** 107–115 (1995).
6. Bartsch, D. *et al.* Aplysia CREB2 represses long-term facilitation: relief of repression converts transient facilitation into long-term functional and structural change. *Cell* **83,** 979–992 (1995).
7. Josselyn, S. A. *et al.* Long-term memory is facilitated by cAMP response element-binding protein overexpression in the amygdala. *J. Neurosci.* **21,** 2404–2412 (2001).
8. Sheng, M. & Greenberg, M. E. The regulation and function of c-fos and other immediate-early genes in the nervous system. *Neuron* **4,** 477–485 (1990).
9. Kelz, M. B. *et al.* Expression of the transcription factor deltaFosB in the brain controls sensitivity to cocaine. *Nature* **401,** 272–276 (1999).
10. Kockel, L., Homsy, J. G. & Bohmann, D. *Drosophila* AP-1: lessons from an invertebrate. *Oncogene* **20,** 2347–2364 (2001).
11. Davis, G. W. & Goodman, C. S. Genetic analysis of synaptic development and plasticity: homeostatic regulation of synaptic efficacy. *Curr. Opin. Neurobiol.* **8,** 149–156 (1998).
12. Zhong, Y., Budnik, V. & Wu, C. F. Synaptic plasticity in *Drosophila* memory and hyperexcitable mutants: role of cAMP cascade. *J. Neurosci.* **12,** 644–651 (1992).
13. Schuster, C. M., Davis, G. W., Fetter, R. D. & Goodman, C. S. Genetic dissection of structural and functional components of synaptic plasticity. Fasciclin II controls presynaptic structural plasticity. *Neuron* **17,** 641–654 (1996).
14. Bailey, C. H., Chen, M., Keller, F. & Kandel, E. R. Serotonin-mediated endocytosis of apCAM: an early step of learning-related synaptic growth in Aplysia. *Science* **256,** 645–649 (1992).
15. Eresh, S., Riese, J., Jackson, D. B., Bohmann, D. & Bienz, M. A CREB-binding site as a target for decapentaplegic signalling during *Drosophila* endoderm induction. *EMBO J.* **16,** 2014–2022 (1997).
16. Zeitlinger, J. *et al.* Defective dorsal closure and loss of epidermal decapentaplegic expression in *Drosophila* fos mutants. *EMBO J.* **16,** 7393–7401 (1997).
17. Karin, M., Liu, Z. & Zandi, E. AP-1 function and regulation. *Curr. Opin. Cell Biol.* **9,** 240–246 (1997).
18. Cheung, U. S., Shayan, A. J., Boulianne, G. L. & Atwood, H. L. *Drosophila* larval neuromuscular junction's responses to reduction of cAMP in the nervous system. *J. Neurobiol.* **40,** 1–13 (1999).
19. Yin, J. C. *et al.* Induction of a dominant-negative CREB transgene specifically blocks long-term memory in *Drosophila*. *Cell* **79,** 49–58 (1994).
20. Osterwalder, T., Yoon, K., White, B. & Keshishian, H. A conditional tissue-specific transgene system using inducible Gal4. *Proc. Natl Acad. Sci. USA* **98,** 12596–12601 (2001).
21. Chang, L. & Karin, M. Mammalian MAP kinase signalling cascades. *Nature* **410,** 37–40 (2001).
22. Riesgo-Escovar, J. R., Jenni, M., Fritz, A. & Hafen, E. The *Drosophila* Jun-N-terminal kinase is required for cell morphogenesis but not for DJun-dependent cell fate specification in the eye. *Genes Dev.* **10,** 2759–2768 (1996).
23. Yang, D. D. *et al.* Absence of excitotoxicity-induced apoptosis in the hippocampus of mice lacking the JNK3 gene. *Nature* **389,** 865–870 (1997).
24. Schwarzschild, M. A., Cole, R. L. & Hyman, S. E. Glutamate, but not dopamine, stimulates stress-activated protein kinase and AP-1-mediated transcription in striatal neurons. *J. Neurosci.* **17,** 3455–3466 (1997).
25. Sagasti, A. *et al.* The CaMKII unc-43 activates the MAPKKK nsy-1 to execute a lateral signalling decision required for asymmetric olfactory neuron fates. *Cell* **105,** 221–232 (2001).
26. Martin-Blanco, E. *et al. puckered* encodes a phosphatase that mediates a feedback loop regulating JNK activity during dorsal closure in *Drosophila*. *Genes Dev.* **12,** 557–570 (1998).
27. DeZazzo, J. *et al.* nalyot, a mutation of the *Drosophila* myb-related Adf1 transcription factor, disrupts synapse formation and olfactory memory. *Neuron* **27,** 145–158 (2000).
28. Stewart, B. A., Atwood, H. L., Renger, J. J., Wang, J. & Wu, C. F. Improved stability of *Drosophila* larval neuromuscular preparations in haemolymph-like physiological solutions. *J. Comp. Physiol. A* **175,** 179–191 (1994).

Acknowledgements

We thank D. Bohmann and E. Hafen for strains, and T. Littleton and H. Bellen for anti-Syt antibodies. We also thank H. Keshishian and T. Osterwalder for sharing *elavGS-GLA4* strains before publication; P. Etter for early assistance; D. Stimson for advice on electrophysiology; and P. Jansma for help with confocal microscopy. We thank P. Etter, R. Narayanan and members of the Ramaswami laboratory for useful discussions and/or comments on the manuscript. The work was funded by grants from the National Institute on Drug Abuse (primarily), the National Institute for Neurological Disorders and Stroke, the Human Frontiers Science Program Organization, McKnight and Alfred P. Sloan Foundations to M.R., and NSF and NIH predoctoral fellowships to C.A.H.

Competing interests statement

The authors declare that they have no competing financial interests.

Correspondence and requests for materials should be addressed to M.R. (e-mail: mani@u.arizona.edu).

Deafness and renal tubular acidosis in mice lacking the K-Cl co-transporter Kcc4

Thomas Boettger*†, Christian A. Hübner*†, Hannes Maier‡, Marco B. Rust*, Franz X. Beck§ & Thomas J. Jentsch*

** Zentrum für Molekulare Neurobiologie, ZMNH, Universität Hamburg, Falkenried 94, 20246 Hamburg, Germany*
‡ HNO Klinik, Universitätsklinikum Eppendorf, Universität Hamburg, Martinistrasse 52, 20246 Hamburg, Germany
§ Physiologisches Institut, Ludwig-Maximilians-Universität München, Pettenkoferstrasse 12, 80336 München, Germany
† These authors contributed equally to this work

Hearing depends on a high K^+ concentration bathing the apical membranes of sensory hair cells. K^+ that has entered hair cells through apical mechanosensitive channels is transported to the stria vascularis for re-secretion into the scala media[1]. K^+ probably exits outer hair cells by KCNQ4 K^+ channels[2,3], and is then transported—by means of a gap junction system connecting supporting Deiters' cells and fibrocytes[4]—back to the stria vascularis. We show here that mice lacking the K^+/Cl^- (K-Cl) co-transporter Kcc4 (coded for by *Slc12a7*) are deaf because their hair cells degenerate rapidly after the beginning of hearing. In the mature organ of Corti, Kcc4 is restricted to supporting cells of outer and inner hair cells. Our data suggest that Kcc4 is important for K^+ recycling[1,5] by siphoning K^+ ions after their exit from outer hair cells into supporting Deiters' cells, where K^+ enters the gap junction pathway. Similar to some human genetic syndromes[6], deafness in *Kcc4*-deficient mice is associated with renal tubular acidosis. It probably results from an impairment of Cl^- recycling across the basolateral membrane of acid-secreting α-intercalated cells of the distal nephron.

Electroneutral K-Cl co-transporters have roles in cell volume regulation, transepithelial transport, and in the regulation of intracellular chloride concentration ($[Cl]_i$). Of the four mammalian K-Cl co-transporters (Kcc1–4), Kcc1 and Kcc3 are broadly expressed, whereas Kcc2 is neurone-specific[7]. In mice lacking Kcc2, the ensuing rise of neuronal $[Cl]_i$ leads to excitatory responses to the normally inhibitory neurotransmitters GABA (γ-aminobutyric acid) and glycine, resulting in spasticity and early postnatal death[8]. Although the coupling of K^+ to Cl^- favours efflux and therefore lowers $[Cl]_i$ under many circumstances, K-Cl co-transporters often operate near electrochemical equilibrium and may also mediate net ion uptake[9].

We have now generated mice constitutively lacking Kcc4 (Supplementary Information Fig. 1a), an isoform with hitherto unknown physiological function. It is predominantly expressed in kidney, heart, lung and liver[10]. Western blots indicated that Kcc4 protein was absent in knockout mice (Supplementary Information Fig. 1c). $Kcc4^{-/-}$ mice were born at the expected mendelian ratio

and were viable and fertile; however, their body weight was roughly 90% of that of their littermates.

Kcc4$^{-/-}$ mice displayed no obvious abnormalities in activity and vision. Vestibular and motor function appeared normal on tilted plates and in rotarod experiments. The absence of acoustic Preyer reflexes in adult mice indicated severe hearing loss. Auditory brainstem responses were recorded from postnatal day 14 (P14) onwards, shortly after mice begin to hear. At this early age, hearing of *Kcc4*$^{-/-}$ mice was normal. It quickly deteriorated during the following week after which mice were nearly deaf, with a hearing loss of 70–80 dB (Fig. 1). Histological analysis revealed that the inner ear developed normally and could not be distinguished from wild-type animals at P14 (Fig. 2a, b). At P21, however, outer hair cells (OHCs) of basal turns of the cochlea (which mediate high frequency hearing) were almost totally lost (Fig. 2c, d), whereas inner hair cells were still present. The degeneration proceeded from basal to apical turns (Supplementary Information Fig. 2). In adult knockout mice, the organ of Corti was lost completely in basal turns (Fig. 2f, h). In apical turns, some hair cells survived, accounting for the residual hearing ability in adult mice (Fig. 1). Probably as a consequence of the loss of hair cells[11], neurons of the cochlear ganglion degenerated as well (Fig. 2h). Even in adult knockout mice, however, there was no collapse of Reissner's membrane, which separates the scala media from the scala vestibuli (Fig. 2g, h). This contrasts with mice where inactivation of transport proteins of the stria vascularis impairs K^+ secretion[11–14], suggesting that Kcc4 is not essential for endolymph production.

Antibodies raised against Kcc4 were used to determine its expression pattern (Fig. 3). At P8, before the onset of hearing, the antibodies stained membranes in the stria vascularis and in almost all cells of the organ of Corti (Fig. 3a). This included the developing epithelial and supporting cells, as well as the membranes of OHCs (Fig. 3c). Outer hair cells were identified by (green) staining for the K^+ channel KCNQ4 (refs 2, 3), which was present in the entire basolateral membrane (Fig. 3c, d). At P14, when the organ has matured to allow hearing, KCNQ4 has reached its adult expression pattern in the basal membrane of OHCs[3] (Fig. 3e, f). At this age, Kcc4 was no longer expressed in hair cells and the stria, but was confined to a subset of supporting cells (Fig. 3b, e, g). Deiters' cells, which support OHCs at their basal pole and whose extensions are interposed between these, were labelled along their entire lateral membranes (Fig. 3e, g). Kcc4 was also present in supporting cells of inner hair cells (Fig. 3g).

K^+ ions enter sensory hair cells from the K^+-rich endolymph through apical mechanosensitive channels. They exit from OHCs presumably through KCNQ4 K^+ channels[2,3] (Fig. 3j). After leaving OHCs, K^+ must be removed, partially by uptake into Deiters' cells. In the potassium recycling model of the inner ear[1,5,15–18], K^+ then diffuses through a gap junction system connecting Deiters' cells to adjacent epithelial cells. After passing through a distinct fibrocyte gap junction system, it then contributes to the K^+ supply for the secretory stria vascularis (Fig. 3j).

The mechanism of K^+ uptake into Deiters' cells has remained unclear. These cells express only very low levels of Na/K-ATPase[18,19]. Their membrane conductance is dominated by a K^+ channel[20]. Owing to its outward rectification, however, the K^+ channel is closed at resting voltages[20], and hence cannot mediate K^+ uptake. Our study suggests that K^+ uptake into Deiters' cells instead occurs through Kcc4. This resembles K^+ uptake by neuronal K-Cl co-transporters, which can buffer the extracellular K^+ concentration ($[K^+]_o$) that can rise during neuronal activity[9]. Similarly, $[K^+]_o$ rises in the tunnel of Corti during sound exposure[21], an effect expected to be even more pronounced in the narrow space between OHCs and Deiters' cells. Unlike active pumping by the Na/K-ATPase, K^+ uptake through Kcc4 would be energetically 'cheap' and would occur close to electrochemical equilibrium. Neither the inflow of K^+ into OHCs through their apical transduction channels, nor its basal efflux through KCNQ4 or its removal by Kcc4 would directly

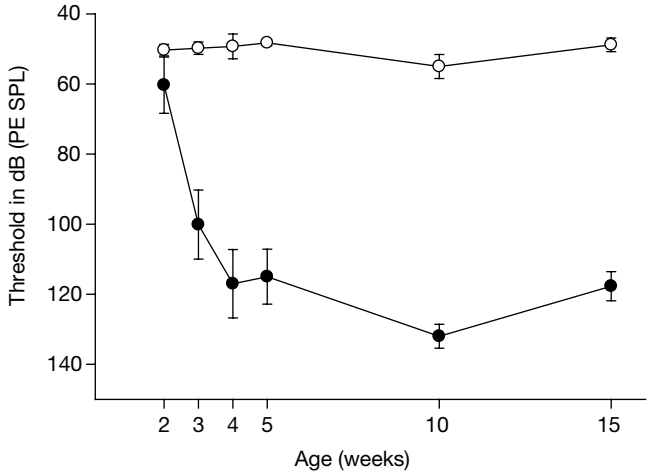

Figure 1 Hearing loss of *Kcc4*$^{-/-}$ mice. Thresholds in peak equivalent sound pressure level (PE SPL; re 20 μPa) of auditory brain stem responses to clicks in wild-type or heterozygous (open circles) and knockout (filled circles) mice of different ages. Vertical bars indicate the standard error of five or more animals.

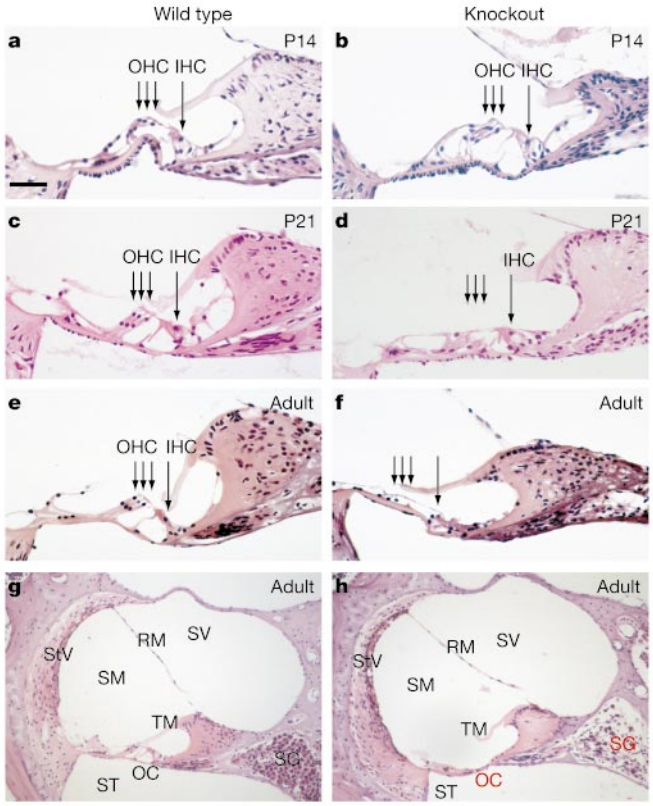

Figure 2 Inner ear morphology by haematoxylin/eosin staining. **a**, **b**, At postnatal day 14 (P14), there is no difference in the organ of Corti between wild-type (**a**) and knockout (**b**) mice. **c**, **d**, At P21, outer hair cells (OHCs) are lost in knockout mice (**d**). **e**–**h**, Adult (3 months of age) cochlea turns reveal normal stria vascularis (StV) and Reissner's membrane (RM), but a loss of OHCs and neuronal degeneration in the spiral ganglion (SG) in the knockout (**f**, **h**) compared with the wild type (**e**, **g**). Three animals per age and genotype gave similar results. IHC, inner hair cell; OC, organ of Corti; SM, scala media; ST, scala tympani; SV, scala vestibuli; TM, tectorial membrane.

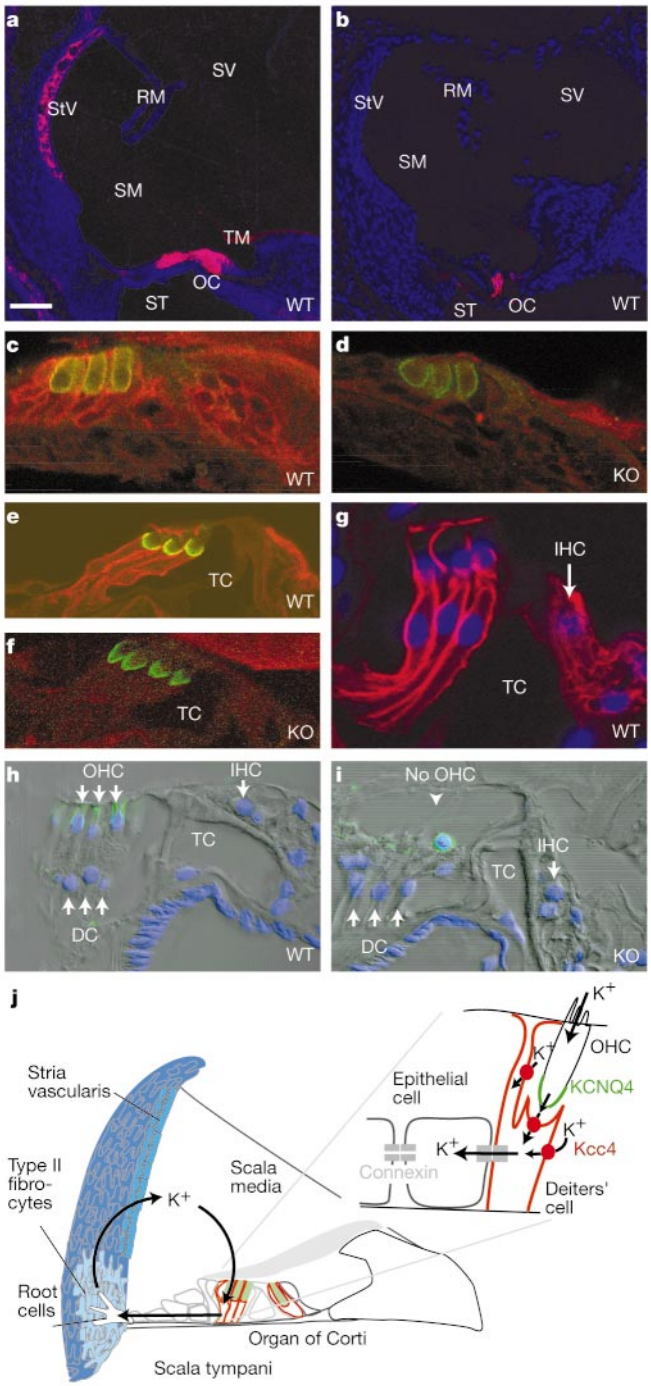

Figure 3 Kcc4 in the cochlea. Abbreviations are the same as in Fig. 2. **a**, **b**, Confocal images of cochlear cross-sections at postnatal day 8 (P8) (**a**) and adult age (**b**) stained for Kcc4 (in red) in the wild type (WT). Nuclei are stained in blue (TOTO-3). **c**, Higher magnification of the organ of Corti at P8 reveals widespread Kcc4 expression. **d**, Kcc4 is absent in the knockout mouse (KO). KCNQ4 (green stain) labels basolateral OHC membranes, which co-stain (yellow) for Kcc4 in the wild type (**c**). **e**, **f**, Cochlea of wild-type (**e**) and knockout (**f**) mice at P14 stained for Kcc4 (red) and KCNQ4 (green). **g**, In the adult wild-type cochlea, Kcc4 (red) is restricted to Deiters' cells and the phalangeal cell enveloping the inner hair cell (nuclei; in blue). **h**, **i**, Organ of Corti in P17 wild-type (**h**) and knockout (**i**) mice stained with the OHC marker prestin (green)[23]. Nuclei are stained blue. Outer hair cells are intact in the organ of Corti in wild-type mice, but are mostly lost in knockout mice. An OHC nucleus left in the organ of Corti of a knockout mouse is surrounded by a shrunken membrane containing prestin (arrowhead). Note intact Deiters' cells. The scale bar in **a** corresponds to 53 μm in **a**, **b**; 12 μm in **c**; 11 μm in **d**, **e**; 25 μm in **f**; 7 μm in **g**; and 13 μm in **h**, **i**. **j**, Model for inner ear K^+ recycling[1,5]. TC, tunnel of Corti.

require metabolic energy. This makes biological sense, as placing the main energy source into the stria vascularis takes metabolic stress away from sensory cells.

The loss of Kcc4 is expected to impede the removal of K^+ ions that have left OHCs. This would change the ionic composition of the small extracellular space that surrounds the basolateral membranes of OHCs, eventually leading to their degeneration. Similarly, mutations in connexin proteins[22] are thought to cause deafness by blocking K^+ removal further downstream at the gap junction level[1]. Deafness caused by *KCNQ4* mutations was attributed to chronic K^+ overload[2,3] by impaired K^+ efflux from OHCs. Importantly, OHCs of *Kcc4*$^{-/-}$ mice degenerated before Deiters' cells were lost (Fig. 3h, i), although Deiters' cells and not OHCs normally express Kcc4 at this stage (Fig. 3e, g). This is consistent with a disturbance of extracellular homeostasis due to impaired salt uptake by Deiters' cells, and may lead to death of OHCs by osmotic stress or membrane depolarization. Furthermore, the degeneration began after the onset

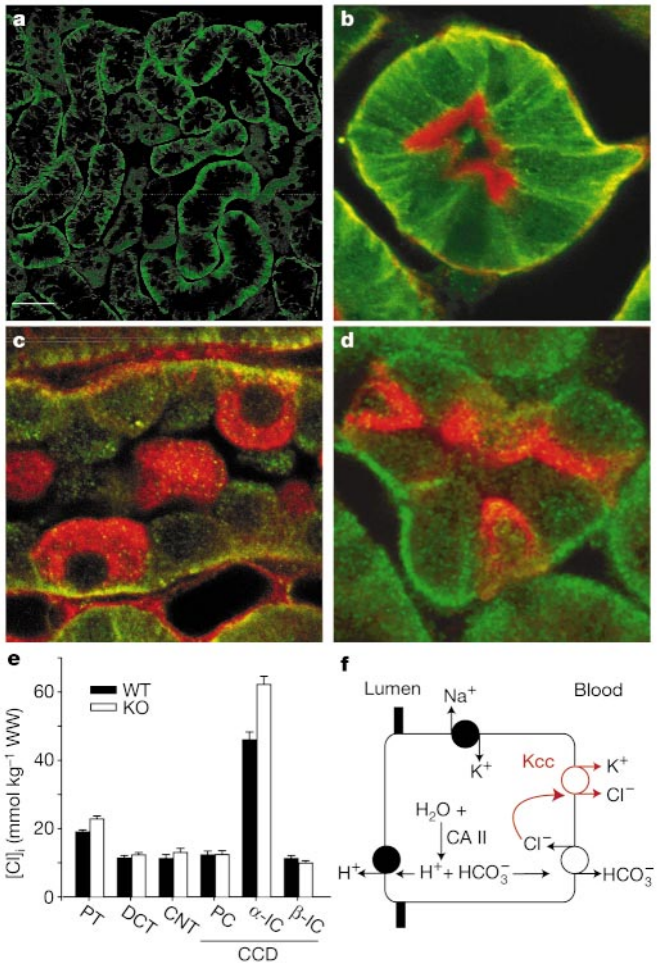

Figure 4 Kcc4 in the kidney. **a**, Overview of Kcc4-stained (green) kidney cortex. **b**, Kcc4 (green) in proximal tubules. Brush borders are stained red by phalloidin. **c**, α-Intercalated cells (identified by red H^+-ATPase staining) of the cortical collecting duct (CCD) express Kcc4 (green). **d**, Basolateral staining of Kcc4 (green) in CCD intercalated cells (which lack aquaporin 2 (red)). The scale bar in **a** corresponds to 31 μm in **a**; 6 μm in **b**; and 5 μm in **c**, **d**. **e**, X-ray microprobe analysis of renal chloride concentrations. In *Kcc4*$^{-/-}$ mice, $[Cl]_i$ (mmol kg^{-1} wet weight) is significantly elevated over wild type in CCD α-intercalated cells (α-ICs) and in proximal tubular (PT) cells. No significant difference was found in distal convoluted tubules (DCT), connecting tubules (CNT), nor in CCD principal cells (PC) or β-intercalated cells (β-ICs). Na^+ and K^+ concentrations were unchanged. Greater than 11 cells of each type were measured (from three animals). WT, wild type; KO, knockout. **f**, Proposed role of Kcc4 in acid secretion by α-intercalated cells.

of hearing, possibly related to the increased K^+ influx through sensory OHCs. Cl^- gradients are important determinants of Kcc4 function, but unfortunately Cl^- transport in the organ of Corti is poorly understood. As crucial aspects of OHC function depend on chloride[23], one may speculate that changes in $[Cl^-]_o$ might contribute to compromising OHC function in *Kcc4*$^{-/-}$ mice.

As in some forms of human syndromic hearing loss[6], deafness in *Kcc4*$^{-/-}$ mice was associated with renal tubular acidosis. The urine of knockout mice was more alkaline than in wild-type littermates (pH 7.3 ± 0.1 (knockout) compared with pH 6.4 ± 0.1 (wild type); $n = 7$ $P < 0.001$), whereas concentrations of Na^+, K^+ and Cl^- were not changed. Consistent with a defect in urinary acidification, blood gas analysis indicated a compensated metabolic acidosis with significantly decreased base excess. Immunofluorescence revealed that Kcc4 is expressed in basolateral membranes of several nephron segments (Fig. 4a–d). Of note, this included α-intercalated cells (Fig. 4c, d). The apical proton ATPase of α-intercalated cells secretes H^+ into the lumen of the distal nephron (Fig. 4f). At the basolateral membrane, acid equivalents are transported by the anion exchanger AE1 (ref. 24). As basolateral HCO_3^- efflux is coupled to Cl^- uptake, Kcc4 may be required for basolateral Cl^- extrusion. Energy-dispersive X-ray microanalysis was used to compare $[Cl]_i$ in renal cells of wild-type and knockout mice (Fig. 4e). $[Cl]_i$ was unchanged in principal cells and in the distal convoluted tubule, which express Kcc4 at low or undetectable levels. By contrast, it was increased in proximal tubules and particularly in α-intercalated cells of knockout mice. High basal $[Cl]_i$ in α-intercalated cells of wild-type mice was described in previous microprobe studies[25], but it should be kept in mind that electron microprobe analysis determines total Cl, not Cl^- activity. Considering the prominent Cl^-/HCO_3^- exchange activity in α-intercalated cells (Fig. 4f), the rise in $[Cl]_i$ predicts a more alkaline intracellular pH in the knockout mouse. This will decrease apical H^+ secretion by increasing the electrochemical gradient against which pumping has to occur. Thus, Kcc4 joins the H^+-ATPase[6] and the AE1 anion exchanger[26] as the third transport protein of α-intercalated cells whose mutation entails renal tubular acidosis.

This work has revealed important and unexpected physiological roles of Kcc4 in the inner ear K^+ transport pathway and in renal acidification. By removing K^+ from the fluid around OHCs, Kcc4 is essential for maintaining the integrity of these sensory cells. In the kidney, Kcc4 is crucial for Cl^- extrusion across the basolateral membrane of acid-secreting α-intercalated cells. As a consequence, the loss of Kcc4 leads to deafness associated with renal tubular acidosis. □

Methods

Disruption of *Kcc4*

Mouse genomic Kcc4 clones were from a 129/SV λ library (Stratagene). MPI2 mouse embryonic stem cells[27] were electroporated with a vector to introduce a neomycin cassette flanked by *loxP* sites (floxed), and a third *loxP* site. Recombinant clones were transfected with a plasmid expressing Cre-recombinase to remove the two exons coding for the first two transmembrane spans of Kcc4 (see Supplementary Information Fig. 1). Mouse lines were established from two independent embryonic stem cell clones. Studies were performed in a mixed 129SV (ref. 27)/C57Bl6 background. We used appropriate littermates as controls.

Antibodies

Polyclonal antibodies were raised against a peptide sequence (EKHRNKDTGPSGFKDC) from the Kcc4 carboxy terminus. Two rabbit sera and one guinea-pig serum proved useful in western blotting and immunofluorescence—they gave identical results. Their specificity was confirmed by analysis of *Kcc4*$^{-/-}$ tissues (Fig. 3c–f; see also Supplementary Information Figs 1c and 4). We also used polyclonal antisera against KCNQ4 (ref. 3), prestin and aquaporin 2 (ref. 28), and the monoclonal antibody E11 against the H^+-ATPase.

Morphology

Mouse kidney and inner ear sections were prepared and analysed by haematoxylin/eosin staining and immunofluorescence as described[29].

Electron microprobe analysis

Kidneys were shock frozen in an isopentane/propane mixture (1:4) at −196 °C. One-micrometre sections were cut on an ultracryomicrotome at −90 °C, and freeze dried. Element concentrations were determined using a scanning transmission electron microscope fitted to an X-ray detector system as described[30].

Hearing tests

Auditory evoked brain-stem responses (ABR) to clicks were recorded in mice anaesthetized with Rompun/Ketanest. Acoustic stimulation and recording of evoked potentials used an Evoselect system (Pilot Blankenfelde). Bioelectric potentials were recorded by subcutaneous silver electrodes at the vertex (reference), forehead (ground), and ventrolateral to the stimulated ear. Acoustic click stimuli were delivered mono-aurally using a Beyer DT-48 earphone, and were monitored with a probe microphone (MK301, Microtech Gefell) integrated into the earpiece. Calibration was done in a 19 μl volume using a second probe microphone (Brüel & Kjær 4135) with a sound-level meter (Brüel & Kjær 2215). Click stimuli had a main component of approximately 200 μs duration and a flat spectra (± 5 dB) with an upper corner frequency of 5.5 kHz. Alternating clicks were applied at a rate of 21 per s and averaged 400–2,000 times.

Urine collection

Mice were kept singly in mouse metabolic cages (PHYMEP) with free access to water and chow. After adaptation to the cage for three days, urine was collected over 24 h periods.

Received 14 December 2001; accepted 15 February 2002.

1. Steel, K. P. & Kros, C. J. A genetic approach to understanding auditory function. *Nature Genet.* **27,** 143–149 (2001).
2. Kubisch, C. *et al.* KCNQ4, a novel potassium channel expressed in sensory outer hair cells, is mutated in dominant deafness. *Cell* **96,** 437–446 (1999).
3. Kharkovets, T. *et al.* KCNQ4, a K^+ channel mutated in a form of dominant deafness, is expressed in the inner ear and the central auditory pathway. *Proc. Natl Acad. Sci. USA* **97,** 4333–4338 (2000).
4. Kikuchi, T., Kimura, R. S., Paul, D. L., Takasaka, T. & Adams, J. C. Gap junction systems in the mammalian cochlea. *Brain Res. Brain Res. Rev.* **32,** 163–166 (2000).
5. Jentsch, T. J. Neuronal KCNQ potassium channels: physiology and role in disease. *Nature Rev. Neurosci.* **1,** 21–30 (2000).
6. Karet, F. E. *et al.* Mutations in the gene encoding B1 subunit of H^+-ATPase cause renal tubular acidosis with sensorineural deafness. *Nature Genet.* **21,** 84–90 (1999).
7. Lauf, P. K. & Adragna, N. C. K-Cl cotransport: properties and molecular mechanism. *Cell Physiol. Biochem.* **10,** 341–354 (2000).
8. Hübner, C. A. *et al.* Disruption of KCC2 reveals an essential role of K-Cl cotransport already in early synaptic inhibition. *Neuron* **30,** 515–524 (2001).
9. Payne, J. A. Functional characterization of the neuronal-specific K-Cl cotransporter: implications for $[K^+]_o$ regulation. *Am. J. Physiol.* **273,** C1516–C1525 (1997).
10. Mount, D. B. *et al.* Cloning and characterization of KCC3 and KCC4, new members of the cation-chloride cotransporter gene family. *J. Biol. Chem.* **274,** 16355–16362 (1999).
11. Vetter, D. E. *et al.* Inner ear defects induced by null mutation of the *isk* gene. *Neuron* **17,** 1251–1264 (1996).
12. Delpire, E., Lu, J., England, R., Dull, C. & Thorne, T. Deafness and imbalance associated with inactivation of the secretory Na-K-2Cl co-transporter. *Nature Genet.* **22,** 192–195 (1999).
13. Dixon, M. J. *et al.* Mutation of the Na-K-Cl co-transporter gene *Slc12a2* results in deafness in mice. *Hum. Mol. Genet.* **8,** 1579–1584 (1999).
14. Lee, M. P. *et al.* Targeted disruption of the *Kvlqt1* gene causes deafness and gastric hyperplasia in mice. *J. Clin. Invest.* **106,** 1447–1455 (2000).
15. Kikuchi, T., Kimura, R. S., Paul, D. L. & Adams, J. C. Gap junctions in the rat cochlea: immunohistochemical and ultrastructural analysis. *Anat. Embryol. (Berl.)* **191,** 101–118 (1995).
16. Spicer, S. S. & Schulte, B. A. Evidence for a medial K^+ recycling pathway from inner hair cells. *Hear Res.* **118,** 1–12 (1998).
17. Wada, J., Kambayashi, J., Marcus, D. C. & Thalmann, R. Vascular perfusion of the cochlea: effect of potassium-free and rubidium-substituted media. *Arch. Otorhinolaryngol.* **225,** 79–81 (1979).
18. Weber, P. C., Cunningham, C. D.III & Schulte, B. A. Potassium recycling pathways in the human cochlea. *Laryngoscope* **111,** 1156–1165 (2001).
19. Spicer, S. S. & Schulte, B. A. Creatine kinase in epithelium of the inner ear. *J. Histochem. Cytochem.* **40,** 185–192 (1992).
20. Nenov, A. P., Chen, C. & Bobbin, R. P. Outward rectifying potassium currents are the dominant voltage activated currents present in Deiter's cells. *Hear. Res.* **123,** 168–182 (1998).
21. Johnstone, B. M., Patuzzi, R., Syka, J. & Sykova, E. Stimulus-related potassium changes in the organ of Corti of guinea-pig. *J. Physiol.* **408,** 77–92 (1989).
22. Kelsell, D. P. *et al.* Connexin 26 mutations in hereditary non-syndromic sensorineural deafness. *Nature* **387,** 80–83 (1997).
23. Oliver, D. *et al.* Intracellular anions as the voltage sensor of prestin, the outer hair cell motor protein. *Science* **292,** 2340–2343 (2001).
24. Rodríguez-Soriano, J. New insights into the pathogenesis of renal tubular acidosis—from functional to molecular studies. *Pediatr. Nephrol.* **14,** 1121–1136 (2000).
25. Beck, F. X., Dörge, A., Giebisch, G. & Thurau, K. Renal excretion of rubidium and potassium: an electron microprobe and clearance study. *Kidney Int.* **34,** 455–462 (1988).
26. Bruce, L. J. *et al.* Familial distal renal tubular acidosis is associated with mutations in the red cell anion exchanger (Band 3, AE1) gene. *J. Clin. Invest.* **100,** 1693–1707 (1997).
27. Voss, A. K., Thomas, T. & Gruss, P. Germ line chimeras from female ES cells. *Exp. Cell Res.* **230,** 45–49 (1997).
28. Nielsen, S., DiGiovanni, S. R., Christensen, E. I., Knepper, M. A. & Harris, H. W. Cellular and subcellular immunolocalization of vasopressin-regulated water channel in rat kidney. *Proc. Natl Acad. Sci. USA* **90,** 11663–11667 (1993).
29. Estévez, R. *et al.* Barttin is a Cl^- channel β-subunit crucial for renal Cl^- reabsorption and inner ear K^+ secretion. *Nature* **414,** 558–561 (2000).

30. Beck, F. X., Schmolke, M., Guder, W. G., Dörge, A. & Thurau, K. Osmolytes in renal medulla during rapid changes in papillary tonicity. *Am. J. Physiol.* **262,** F849–F856 (1992).

Supplementary Information accompanies the paper on *Nature's* website (http://www.nature.com).

Acknowledgements

We thank J. Faulhaber and H. Ehmke for blood gas analysis; M. Bösl for blastocyst injection and implantation; M. Knipper for the prestin antiserum; M. Knepper for the aquaporin 2 antiserum; S. Gluck for the proton ATPase antiserum; M. Kolster, B. Dierkes and I. Öztürk for technical assistance; H. Voss for taking care of animals; and U. Koch for support. This work was supported by grants from the Deutsche Forschungsgemeinschaft, the Fonds der Chemischen Industrie, and the Prix Louis-Jeantet de Médecine to T.J.J.

Competing interests statement

The authors declare that they have no competing financial interests.

Correspondence and requests for materials should be addressed to T.J.J. (e-mail: jentsch@zmnh.uni-hamburg.de).

Structural determinants for GoLoco-induced inhibition of nucleotide release by Gα subunits

Randall J. Kimple*, Michelle E. Kimple†, Laurie Betts*†, John Sondek*†‡ & David P. Siderovski*‡§

** Department of Pharmacology; † Department of Biochemistry and Biophysics; ‡ Lineberger Comprehensive Cancer Center; and § UNC Neuroscience Center, The University of North Carolina at Chapel Hill, Chapel Hill, North Carolina 27599, USA*

Heterotrimeric G-proteins bind to cell-surface receptors and are integral in transmission of signals from outside the cell. Upon activation of the Gα subunit by binding of GTP, the Gα and Gβγ subunits dissociate and interact with effector proteins for signal transduction. Regulatory proteins with the 19-amino-acid GoLoco motif[1,2] can bind to Gα subunits and maintain G-protein subunit dissociation in the absence of Gα activation[3–7]. Here we describe the structural determinants of GoLoco activity as revealed by the crystal structure of $G\alpha_{i1}$–GDP bound to the GoLoco region of the 'regulator of G-protein signalling' protein RGS14. Key contacts are described between the GoLoco motif and Gα protein, including the extension of GoLoco's highly conserved Asp/Glu-Gln-Arg triad into the nucleotide-binding pocket of Gα to make direct contact with the GDP α- and β-phosphates. The structural organization of the GoLoco–$G\alpha_{i1}$ complex, when combined with supporting data from domain-swapping experiments, suggests that the Gα all-helical domain and GoLoco-region carboxy-terminal residues control the specificity of GoLoco–Gα interactions.

In heterotrimeric G-protein signalling, cell surface receptors (GPCRs) are coupled to membrane-associated heterotrimers comprising a GTP-hydrolysing Gα subunit and a Gβ–Gγ dimer. Gβγ binds tightly to GDP-bound Gα, enhancing the coupling of Gα to the receptor and acting as a guanine nucleotide dissociation inhibitor (GDI) to inhibit spontaneous GDP release[8,9]. Agonist-promoted exchange of bound GDP for GTP alters the conformation of three Gα 'switch' regions (I–III) and allows Gβγ dissociation and subsequent effector interactions by both α·GTP and free Gβγ. Intrinsic, or RGS protein-accelerated[10], GTP hydrolysis by Gα returns the subunit to the GDP-bound state and allows Gαβγ re-assembly and termination of effector interactions. GoLoco-motif proteins interact specifically with GDP-bound $G_{i/o}$-class Gα subunits, preventing both GDP release[3–6] and Gβγ re-assembly[6,7], and thus permitting continued Gβγ–effector interactions in the absence of Gα activation[2]. The GoLoco motif is present in RGS12, RGS14, LOCO, Purkinje-cell protein-2 (Pcp2) and Rap1GAP isoforms, and is repeated in tandem arrays within the *Drosophila* protein Rapsynoid (also known as Partner of Inscuteable, Pins) and its mammalian homologues AGS3 and LGN (ref. 1). During development of the *Drosophila* nervous system, the binding of Pins to $G\alpha_i$, and the resultant displacement of Gβγ, is thought to underlie mitotic spindle re-orientation, which is critical for the asymmetric cell divisions exhibited by embryonic neuroblasts and sensory organ precursor cells[7]. More recently, the Pins-related protein LGN has been shown to be essential for mitotic spindle assembly and organization in mammalian cells[11].

To ascertain the structural determinants of selective α·GDP binding and novel GDI activity exhibited by GoLoco proteins, we determined the crystal structure of the RGS14 GoLoco region bound to an adenylyl cyclase-inhibitory Gα subunit (α_{i1}·GDP). Diffraction data collected from a single crystal at 100 K were used to refine the structure to 2.7 Å resolution (Supplementary Information Table A) using the structure of α_{i1}·GDP·Mg^{2+} as a model for molecular replacement[12].

Of the 36 amino acids of the R14GL peptide (residues r496–r530, numbered according to full-length rat RGS14), 35 are ordered

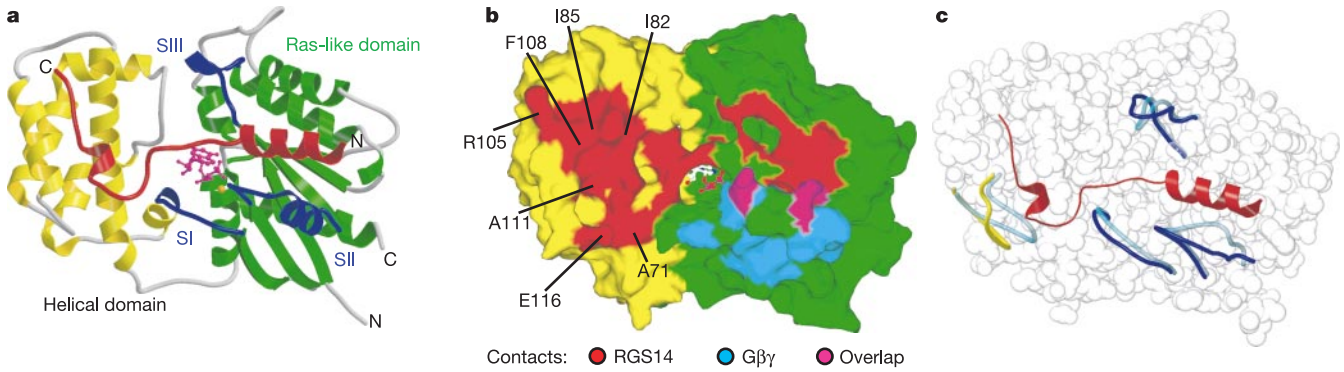

Figure 1 α_{i1}·GDP in complex with the RGS14 GoLoco region. **a**, Ribbon drawing of R14GL peptide (red) in contact with the Ras-like (green) and all-helical (yellow) domains of $G\alpha_{i1}$. Also shown are the three switch regions of $G\alpha_{i1}$ (blue), GDP (magenta) and Mg^{2+} (orange). **b**, Molecular surface of R14GL (red) and Gβγ (cyan) contacts on $G\alpha_{i1}$·GDP, denoting shared switch II residue contacts (magenta). Highlighted are $G\alpha_{i1}$ residues that contact the R14GL peptide and are different within $G\alpha_o$. **c**, Space fill model of α_{i1}·GDP in its R14GL-bound conformation (switch regions in blue, αB–αC loop in yellow) and $G\beta\gamma_{2}$-bound conformation (in cyan).